Concomitant Emergence of Circularly Polarized Luminescence and Single-Molecule Magnet behavior in chiral-at-metal Dy complex

Bahjat El Rez,[a] Jiawen Liu,[c] Virginie Béreau,[a,b] Carine Duhayon,[a] Yuki Horino,[d] Takayoshi Suzuki,[d,e] Laurent Coolen,*[,c] Jean-Pascal Sutter*[,a]

[a] Laboratoire de Chimie de Coordination du CNRS (LCC-CNRS), Université de Toulouse, CNRS, Toulouse, France
sutter@lcc-toulouse.fr
[b] Université de Toulouse, Institut Universitaire de Technologie-Département de Chimie, Castres, France
[c] Sorbonne Université, CNRS, Institut de NanoSciences de Paris, INSP, F-75005 Paris, France
coolen@insp.jussieu.fr
[d] Graduate School of Natural Science and Technology, Okayama University, Okayama 700-8530, Japan.
[e] Research Institute for Interdisciplinary Science (RIIS), Okayama University, Okayama 700-8530, Japan

Abstract:

Circularly polarized luminescence (CPL) was evidenced for the first time in single crystals of a chiral-at-metal Dy(III) single-molecule magnet. This CPL is opposite for the enantiomers and was found to appear and become stronger at lower temperatures when the relaxation of the magnetization for the Dy centers is slower. The luminescence dissymmetry factor (g_{lum} up to +/-0.18) was found to have little dependence on the emission angle which permitted observing a similar CPL for an ensemble of micro-crystals of random orientations. The investigated Dy(III) compounds consist of bimetallic ZnLn units assembled by a Schiff base ligand, control of the stereochemistry of the Ln center was achieved using chiral [3-(trifluoromethylhydroxymethylene)-camphorate]$^-$ as anionic ligands. CPL was not found for the Eu(III) homologues.

Graphical abstract:

Circularly polarized luminescence was evidence in solid state for a chiral-at-metal Dy(III) single-molecule magnet. This CPL is opposite for the enantiomers and develops at lower temperatures when the relaxation of the magnetization for the Dy becomes slower.

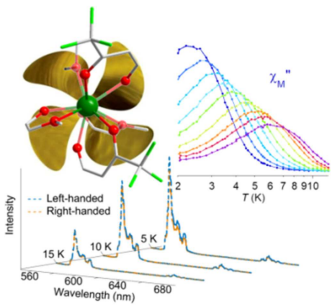

INTRODUCTION

Single-molecule magnets (SMM) and single-chain magnets (SCM) are the focus of a tremendous interest because of their prospective interest as active magnetic materials in future devices. These discrete and 1–D spin architectures are characterized by a possible blocking of their magnetization below a critical temperature which confers them bistability property.[1] Remarkable progress has been achieved in the design of such species and in the understanding of their physics. An emerging target concerns their implementation as active materials in demonstrators, an aspect that requires addressing the readout of the orientation of their magnetization. The synergy that can exist between magnetic and optical properties offers interesting possibilities.

The interplay between light and magnetism has remained a continuous research interest since the seminal report by Faraday in 1845[2] of a rotation by a magnetic field of the plane of polarization of light propagating in a dielectric material. More generally, magneto-optical effects rely on a change of light polarization or intensity when propagating through a medium that is altered by the presence of a magnetic field.[3] An interesting situation arises when the propagating medium is chiral and magnetized which results in the emergence of novel properties called magneto-chiral dichroism (MChD) in absorption and magneto-chiral birefringence in refraction.[4-7] The simultaneous breaking of space and time-inversion symmetries leads to a slight difference in the optical absorption coefficient of the medium when the magnetic polarization of the material is parallel or antiparallel to the propagation of non-polarized light, (i.e. $\varepsilon^{\uparrow\uparrow} - \varepsilon^{\uparrow\downarrow} \neq 0$).[8] The observed magneto-chiral dichroism will reverse sign on changing the enantiomer of the chiral medium. The same situation applies for light emitted by a luminescent chiral material.[9, 10] MChD has been evidenced in chiral magnets and chiral paramagnetic compounds, and was shown to be enhanced by the intrinsic magnetic field of the medium, especially by magnetic ordering. [11-13]

Circular polarization of luminescence induced by a magnetic field (MCPL)[14] is another magneto-optical effect. It corresponds to a difference in intensities of the left-handed and right-handed circularly polarized components of the emitted light. Interestingly, chiral compounds can exhibit circularly polarized luminescence (CPL) even in absence of magnetic field. [15, 16] Like for MChD, MCPL intensity is stronger for ferromagnetic-like materials[17] but the effect of intra-material magnetization on CPL remains poorly addressed. CPL can be especially strong for chiral lanthanide(III) complexes in solution.[15] Few reports have analyzed solid-state lanthanide CPL whereas some results suggest CPL may be increased in solid-state crystals as compared to solutions.[18, 19] Opto-electronic applications such as 3D-display, open-space secure communications or anti-counterfeiting may benefit from solid-state CPL sources.

Herein we report on circularly polarized luminescence exhibited by single crystals of a chiral-at-metal Dy(III) single-molecule magnet. This CPL is opposite for the enantiomers and was found to appear and become stronger at lower temperatures when the relaxation of the magnetization for the Dy centers is slower. Such CPL was not observed for the isostructural Eu(III) complexes with non-magnetic ground state.

RESULTS AND DISCUSSION

The Dy(III) compounds investigated consist of bimetallic ZnLn units assembled by a Schiff base ligand (H_2L^{Me2}, Scheme 1). Such ZnDy derivatives are known to exhibit SMM behavior[20-23] but also to be good luminophores.[24] For an electronic transition to possess an associated CPL, it must occur in the presence of a chiral force field; in other words the luminescent metal ion must be center of chirality. This was achieved using chiral [3-(trifluoromethylhydroxymethylene)-camphorate] (camph$^-$ hereafter) as anionic ligand for the Ln center.

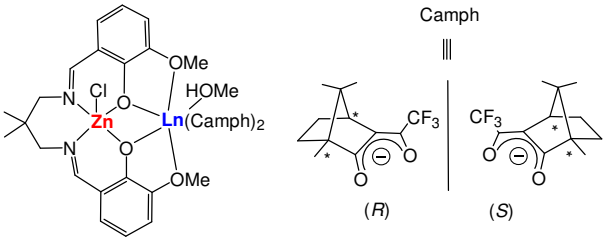

Scheme 1: Sketch of the ligand system in [L^{Me2}Zn(Cl)Ln(camph)$_2$(MeOH)]

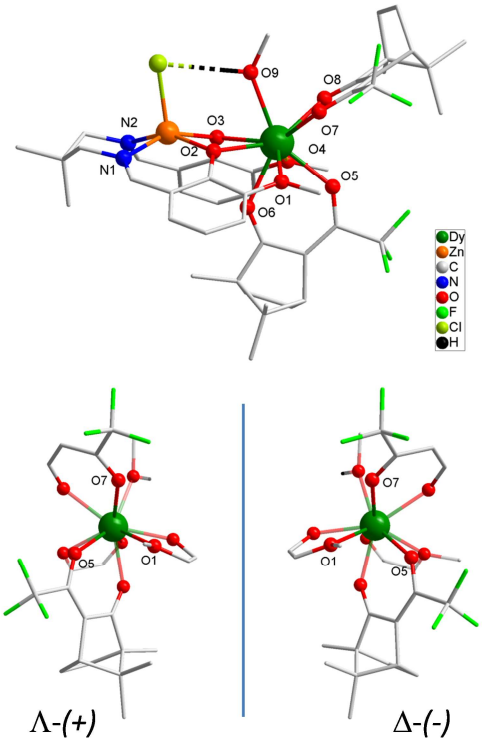

Figure 1. *(top)* [L^{Me2}Zn(Cl)Dy(*(-)*-camph)$_2$(MeOH)], **Δ-Dy**, and *(bottom)* coordination sphere of the Dy(III) in both enantiomers (for clarity only one chiral camph ligand is depicted).

[L^{Me2}Zn(Cl)Dy(*(+)*-camph)$_2$(MeOH)], **Λ-Dy**, was formed by reaction of $DyCl_3(H_2O)_6$, $ZnL^{Me2}\cdot 2H_2O$, *(+)*-3-(trifluoroacetyl)camphor, and piperidine in 1/1/2/2 ratio in MeOH, whereas its enantiomer **Δ-Dy** was obtained with *(-)*-3-(trifluoroacetyl)camphor. Same procedure was followed to prepare the isomorphous Eu-enantiomers **Λ-Eu** and **Δ-Eu**, and the mixed metal complex **Λ-Dy/Y** (see Experimental section).

Crystals formed by slow evaporation of solvent (Picture S1) crystallize in monoclinic space group $P2_12_12_1$ and asymmetric unit comprises a single complex. The molecular structure for **Δ-Dy** is depicted in Figure 1 (Figure S1 for stereo-isomer **Λ-Dy**, Figure S2 for **Λ-Eu**, and Figure S3 for the mixed metal **Λ-Dy/Y** derivative; selected bond distances are given in Table S2). It consists of a bimetallic complex made of the Schiff base accommodating a Zn(II) ion and a Dy(III) ion in the [N2O2] and [O2O2] compartments, respectively. The Zn(II) is in a square-base pyramid-like environment with two oxygen and two nitrogen atoms of the Schiff base in the basal position and one Cl atom in the apical position. The Dy center, in addition to the four oxygen atoms of the Schiff base, is associated with two $Camph^-$ ligands in chelate interaction with the Ln ion, and one MeOH molecule. An intramolecular hydrogen bond is established between the OH group of the alcohol and the Cl atom. The polyhedral shape of the Dy coordination sphere can be described either by a distorted capped square antiprism or a distorted muffin geometry (Table S3).[25] The Ln is a stereogenic center and its formation is stereospecific; the Λ conformation is obtained by coordination of *(+)*-$camph^-$ whereas enantiomer Δ is achieved with *(-)*-$camph^-$ ligands (Figure 1). The enantiomorphism of the two derivatives is confirmed by their solid state circular dichroism (CD) spectra showing symmetrical signals but of opposite sign (figure 2). The CD transitions can be assigned to π-π* intra-ligand transitions of the Schiff-base moiety (see Figure S4).[26]

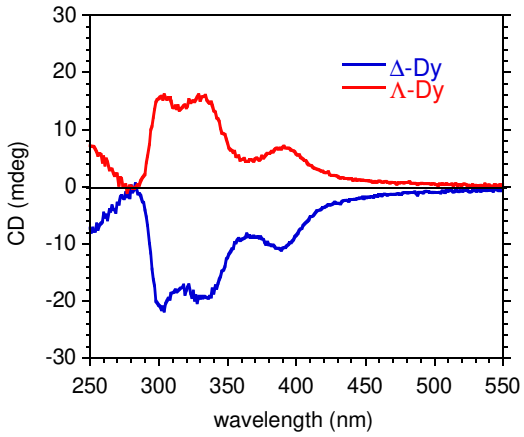

Figure 2. Solid state CD spectra for **Δ-Dy** (in blue) and **Λ-Dy** (in red)

These complexes were found to exhibit slow relaxation of their magnetization. AC susceptibility revealed the emergence of an out-of-phase component, χ_M'', below 12 K in zero field with however, clear contribution of quantum tunneling of the magnetization (QTM) for lower temperatures. This QTM is only partly quenched by a static field (Figure S5) therefore the dilution technique was applied to investigate the relaxation characteristics. The behavior for **Λ-Dy** diluted (9 %) in an isostructural diamagnetic matrix of [L^{Me2}Zn(Cl)Y(*(+)*-camph)$_2$(MeOH)], i.e. **Λ-Dy/Y**, is given in Figures 3 and S6. AC susceptibility data were collected in a static field of 1 kOe found to be the optimal field to reach slowest relaxation. Analysis of the Cole-Cole plots (Figure S6d) revealed a rather narrow distribution

width of the relaxation in the higher *T* range (10.5-7 K) with α = 0.15. For lower *T* the value of α steadily increased to 0.4 for 2, K which is indicative of a multi-process relaxation.

The temperature dependence of the relaxation time (Figure S6c) was obtained by analyzing the χ_M'' = $f(\nu)$ for different temperatures with an extended Debye model. The linear variation of $\tau = f(1/T)$ between 8.5 and 4 K was fitted assuming a thermally activated process yielding U_{eff}/k_B = 25 K with τ_0 = 7.4x10^{-6} s. A modelling over the entire temperature range (2 to 8.5 K) was possible assuming contributions from the Orbach, Raman and direct relaxation processes ($\tau = \tau_0 e^{Ueff/kT} + 1/(RT^n) + 1/(DH^4T)$. The values of the adjustment parameters are U_{eff}/k_B = 23 (± 3) K, τ_0 = 1 (± 2) x10^{-5} s, R = 0.1 (± 0.6) s^{-1}, n = 4 (± 7), D = 2 (± 2) x10^4 K^{-1}T^{-4}s^{-1}). The value for τ_0 is obviously too large for an Orbach process but calculation uncertainty is large because of the number of variables. Adjustment to the experimental data failed without the Orbach contribution. These results confirm the emergence of slow relaxation of the magnetization below 12 K for probing frequency of 1 kHz.

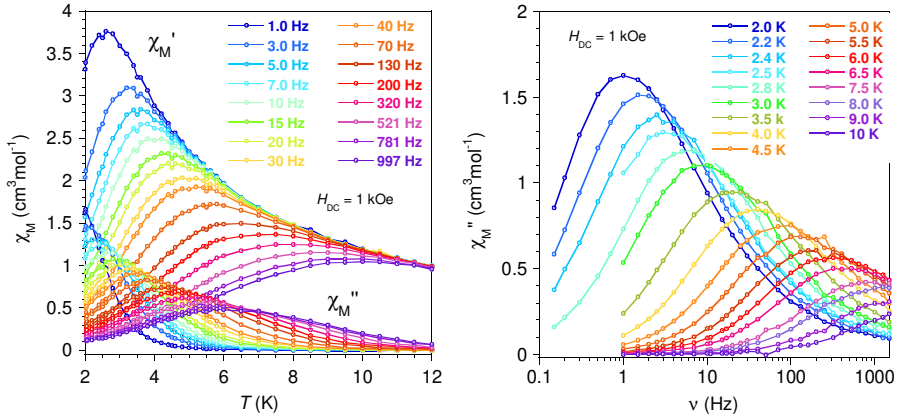

Figure 3. AC susceptibility behavior for **Λ-Dy** diluted in diamagnetic [L^{Me2}Zn(Cl)Y(*(+)*-camph)$_2$(MeOH)].

The luminescence properties of individual crystals of **Λ-Dy** and **Δ-Dy** were investigated by low temperature (5 - 30 K) micro-photoluminescence. We excited an area of 30 µm diameter so that single monocrystals could be observed (Picture S2). Figure 4 shows the emission spectra for a **Λ-Dy** crystal along left-handed and right-handed circular polarizations. Two groups of emission peaks appear at 573 and 663 nm and are attributed respectively to the $^4F_{9/2}$-$^6H_{13/2}$ and $^4F_{9/2}$-$^6H_{11/2}$ transitions of Dy(III).[27, 28] The emission intensity decreases as a function of temperature, barely any emission being observed above 30 K. For both transitions, the left-handed circularly-polarized emission is slightly stronger than the right-handed polarization. This observation was made for all observed **Λ-Dy** crystals. On the other hand, for all **Δ-Dy** crystals the right-handed emission was consistently stronger than the left-handed emission (Figure S7). The degree of circular polarization is usually quantified by the luminescence dissymmetry factor g_{lum} (Equation 1).[15]

$$g_{lum} = \frac{I_L - I_R}{\frac{1}{2}(I_L + I_R)} \qquad (1)$$

This quantity ranges between -2 and +2 and vanishes when the emission is not circularly polarized. It is typically of the order of 10^{-3} – 10^{-2} for chiral organic molecules but can reach higher values for lanthanide complexes,[15] with up to g_{lum} ≈ 1.4 reported for Eu(III).[29, 30] For solutions of Dy(III) chiral complexes, generally lower g_{lum} values of 0.01[27] and up to ≈ 0.4[31] have been achieved.

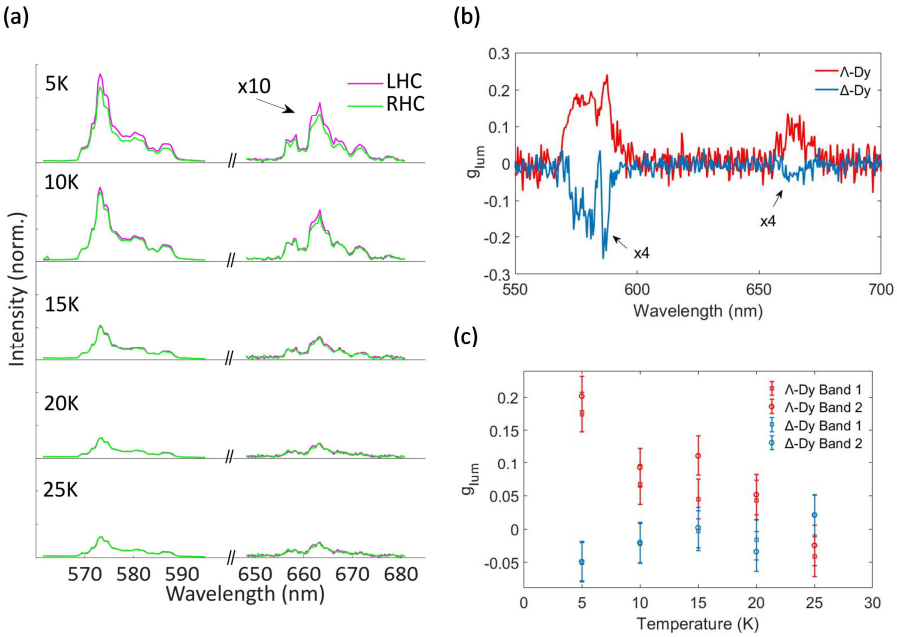

Figure 4. Temperature dependent emission of **Λ-Dy** crystal. (a) Purple lines: left-handed circular (LHC) polarization; green lines: right-handed circular (RHL) polarization for the **Λ-Dy** sample at different temperatures ; (b) CPL dissymmetry factor g_{lum} as a function of the wavelength for the two samples at 5 K; (c) Temperature-dependent variation of the luminescence dissymmetry factor, g_{lum} for the two samples and the two spectral bands.

From our spectra, using equation 1, we extract the dissymmetry factor as a function of the wavelength (fig. 4(b)) for the two samples at 5 K. Over the two emission spectral intervals, the dissymmetry factor shows unambiguous opposite signs for the two samples, demonstrating the effect of the ligand chirality on the CPL. The dissymmetry factor is quite lower in absolute value for the **Δ-Dy** sample, possibly because of some measurement uncertainty. We then average the dissymmetry factor over each of the two intervals and plotted its average value as a function of the temperature in figure 4(c) and S7. In spite of some uncertainty on g_{lum} values and some variation between the individual crystals, a general trend is observed: the degree of circular polarization decreases with temperature and vanishes around 25 K. These observations were repeated for several crystals, with a distribution of g_{lum} values ranging between 0.04 and 0.18 for **Λ-Dy** and between -0.04 and -0.16 for **Δ-Dy** at 5 K.

It can be noticed that the appearance of CPL and the increase of g_{lum} with decrease of temperature coincide with the emergence of slow relaxation of magnetization for these complexes. As mentioned above, CPL can be induced by the chiral structure of the luminophore but it can also be generated by a magnetic field whether applied or intrinsic to the material. For a SMM, the later results from the easy-axis orientation the individual magnetization. In order to provide additional information on the possible role of each of these sources, studies have been carried out on isomorphous Eu(III) complexes (see SI for crystal data). At low temperature, Eu(III) is essentially non-magnetic, which makes it possible to probe the contribution of structural origin. Moreover, Eu(III) is the lanthanide element for which the strongest CPL has been reported in the literature.[15, 27, 31]

Characteristic luminescence bands where observed below 250 K for Λ-**Eu** and Δ-**Eu** (Figure S8). It can be noticed that the most prominent emission is arising from the $^5D_0$ -> $^7F_2$ transition with two main lines (613 and 619 nm) for each enantiomer, whereas the intensity of the $^5D_0$ -> $^7F_0$ transition at 585-595 nm is weak. Their relative intensity ratio is R = 19. This feature is characteristic for a low symmetry field at the Eu(III) site, in agreement with point symmetry *C*s deduced from the crystal structure (Table S3).[32, 33] Down to 5 K the emission is exactly the same for the two circular polarizations. The degree of circular polarization was calculated for each peak at each temperature and g_{lum} was always close to 0, fluctuating between -0.04 and +0.04. It can be concluded that CPL of structural origin is very low for these compounds.

Finally, we used Fourier-plane imaging to obtain the emission angular distribution in the two circular polarizations (Figure 5) for a **Λ-Dy** and a **Δ-Dy** crystal. The overall emission is distributed rather isotropically for the first crystal and has more preferred directions for the second crystal, probably due to the different shape of the crystal boundaries, but for both crystals the angular distribution is the same for the two emission lines. In spite of some significant noise, the curves clearly show that the degree of circular polarization has little dependence on the emission angle. This is confirmed by observing an ensemble of crystals of random orientations. A powder formed by crushing a single crystal and illuminated over a 30 µm diameter area showed dissymmetry factors of the same order as for a single crystal, also with isotropic angular distribution (Figure S9). There is thus little difference between the circular-polarization of a single crystal and an ensemble of randomly-oriented crystals. Beyond the obvious advantage for processing such a material, the use of a powder also solves the problem of the amount of material needed for reliable measurement.

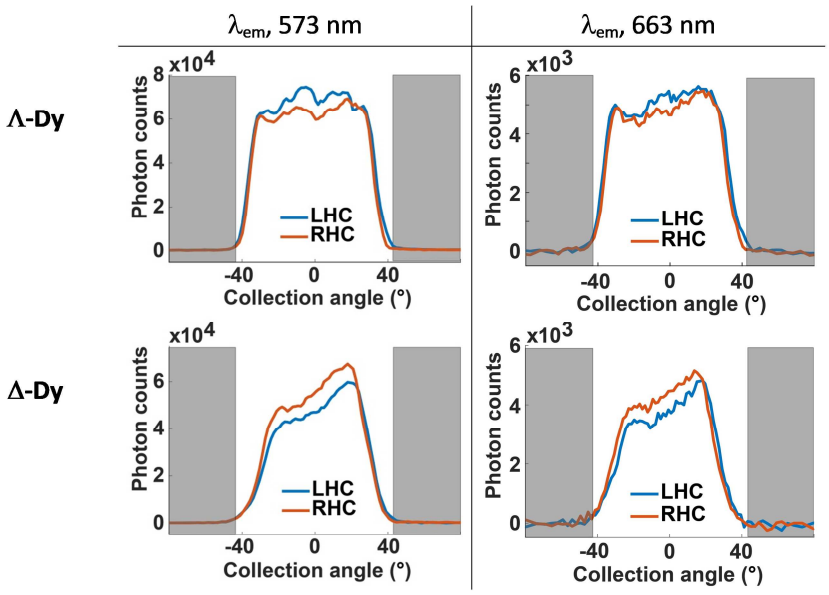

Figure 5. Angular distribution of the emission bands at 573-nm and 663-nm bands for a (top) **Λ-Dy** and (bottom) a **Δ-Dy** crystal at 5 K. Angular range scanned is +/- 44°. The grey portions correspond to the angles not collected by the objective (outside the numerical aperture)

CONCLUDING REMARKS

Concomitant rise of circularly polarized luminescence and SMM-type behavior was evidenced in the solid state for an enantiomeric pair of chiral Dy complexes. This observation strongly suggests that magnetic anisotropy of the Dy combines with structural chirality to enhance the chiral force field acting on the luminescent Ln center. The synergy between the emission and the magnetic features is supported by the lack of CPL for the Eu derivatives. This allows excluding a purely structural effect and substantiates the essential role of the magnetization blocking in the CPL observed for the Dy complexes.

It is noticeable that the observed luminescence dissymmetry factor is large with $|g_{lum}|$ up to 0.18. Interestingly, the same CPL was found for singles crystals and the polycrystalline powders. This is a particularly important observation as it suggests that CPL can be exploited on a crystalline powder and is not limited to a single crystal.

EXPERIMENTAL

General procedures: Reagents and solvents were obtained commercially and used without further purification. The Schiff base H_2L^{Me2} and its Zn complex $[ZnL^{Me2}]\cdot 2H_2O$ were prepared as previously reported[34] and recrystallized from MeOH solutions by slow evaporation of the solvents. Purity of the samples was verified by ^{1}H NMR and elemental analysis. The two enantiomers (+) and (-) of the trifluoroacetyl-3-camphor were synthesized following the literature procedure.[35] Purity of the samples was checked by ^{1}H, ^{13}C, ^{19}F NMR, and by specific optical rotation measurements. Elemental C, H and N analyses were performed on a Perkin-Elmer 2400 II analyzer on freshly prepared and isolated samples. IR spectra were recorded in the 4000-700 cm^{-1} range with a Perkin-Elmer Spectrum 100 FTIR using the ATR mode. Optical rotation measurements were performed on a Perkin-Elmer 241 polarimeter with a sodium lamp, at room temperature. ^{1}H NMR spectra were recorded using a DPX300 Brüker spectrometer with working frequencies at 300 MHz for ^{1}H. Chemical shifts were referenced to the residual proton resonance of the deuterated solvents.

Magnetic studies: Magnetic measurements were carried out with a *Quantum Design* MPMS 5S SQUID magnetometer. Magnetic susceptibility, χ_M, between 2 and 300 K was obtained with an applied field of 1000 Oe. Isothermal magnetization measurements were performed up to 5 T at 2 K. The *ac* susceptibility responses were recorded using an oscillating field of H_{AC} = 3 Oe in zero field and under applied static field of 0.1T. The measurements were performed on crushed crystals from freshly isolated samples mixed to grease and held in gelatin capsules. The molar magnetic susceptibilities were corrected for sample holder and for the diamagnetic contribution of all the atoms by using Pascal's tables.[36]

Solid-state Circular Dichroism (CD) measurement: The solid-state CD spectra (collected in transmittance mode) were measured on a JASCO J-720 spectropolarimeter using KBr disks of samples. A disk was prepared from several crystals of a batch of either **Δ-Dy** or **Λ-Dy** enantiomer with crystalline KBr, according to the following procedure: A mixture of sample and KBr was well ground in an agate mortar then vacuum pressed to form a uniform disk. The disk was placed in a sample holder, which was then positioned in the cell holder of the spectropolarimeter.[37] For each disk, the CD signals were measured from both sides, and the average was taken. A blank disk was used to measure background spectra. The data were corrected accordingly.

Crystallographic Studies. Data collections were performed at low temperature on a Bruker Apex2 (Mo microfocus source) or an Oxford-Diffraction Gemini (Cu source) diffractometer. The structures were solved by SUPERFLIP[38] or SIR92,[39] and refined by means of least-squares procedures on *F or F²* using the programs of the PC version of CRYSTALS.[40] For mixed metal compound **Λ-Dy/Y** best agreement was obtained for ratio 0.16 Dy/0.84. Atomic scattering factors were taken from the International tables for X-ray Crystallography. Hydrogen atoms were refined using a riding model. The absolute configuration of the compounds was determined unambiguously by Flack parameter refinement. Data are gathered in table S1. Cif have been deposited at CCDC under references 2007104 (for **Δ-Dy**), 2007105 (for **Λ-Dy**), 2018680 (for **Λ-Eu**), and 2033959 (for **Λ-Dy/Y**).

CPL studies: Crystals of size 300-800 µm were attached by a silver lacquer to the cold finger of a helium-flow cryostat (Oxford, HiRes II) and observed by a homemade microscope (0.7 numerical aperture objective, x60 magnification). The sample was illuminated through the objective by the light from a mercury lamp filtered over a 330-480 nm pass band. The fluorescence emission was collected by the same objective, filtered by a 500 nm long-pass filter and analyzed by an imaging spectrometer (Horiba Jobin-Yvon, Triax-190). Circular polarization analysis was performed by introducing a polarizer before the spectrometer entrance and comparing the +45° and -45° positions of a quarter-wave plate before the polarizer.

The polarization effect of the different setup elements was corrected by introducing compensating elements. Fluorescent polymer spheres (Thermo Fisher, 200nm, 580-605 nm emission) were used for setup polarization calibration. By circular polarization analysis, an average degree of circular polarization of 0 was measured, with fluctuation in the range of ±0.02. When introducing a polarizer below the objective to polarize the emission, a 0.99 degree of linear polarization was obtained. We thus conclude that the emission polarization was preserved by the setup with 1-3 % precision.

Syntheses:

[L^{Me2}Zn(Cl)Dy(*(+)*-camph)$_2$(MeOH)], **Λ-Dy**, and [L^{Me2}Zn(Cl)Dy(*(-)*-camph)$_2$(MeOH)], **Δ-Dy**: [ZnL^{Me2}]·2H_2O (233 mg; 0.5 mmol) and $DyCl_3$·6H_2O (188 mg; 0.5 mmol) were solubilized in 10 mL of methanol. Either the *(+)*-3-(trifluoroacetyl)camphor or *(-)*-3-(trifluoroacetyl)camphor (250 mg; 1 mmol) was added to this solution followed by piperidine (85 mg; 1 mmol). The resulting pale yellow solution was stirred at room temperature for 30 min. and then transferred in a crystallization tube for slow evaporation of the solution. Pale yellow crystals suitable for X-Ray diffraction appeared after a few days (**Picture S1**). They were collected and washed with methanol.

Data for **Λ-Dy**: Yield 410 mg (71 %). IR (ATR): ν = 3251 (w), 2955 (m), 1652 (s), 1639 (s), 1535 (m), 1473 (m), 1424 (m), 1392 (w), 1293 (m), 1267 (m), 1243 (w), 1222 (vs), 1200 (vs), 1178 (s), 1126 (s), 1069 (s), 1053 (m), 1023 (m), 972 (m), 918 (w), 850 (m), 803 (w), 734 (s), 642 (m) cm^{-1}. $C_{46}H_{56}ClDyF_6N_2O_9Zn$ (1158.3): calcd. C 47.70, H 4.87, N 2.42; found C 47.46, H 4.80, N 2.30.

Data for **Δ-Dy**: Yield 355 mg (61 %). IR (ATR): ν = 3252 (w), 2955 (m), 1652 (s), 1640 (s), 1539 (m), 1472 (m), 1423 (m), 1393 (w), 1295 (m), 1268 (m), 1244 (w), 1221 (vs), 1201 (vs), 1179 (s), 1127 (s), 1069 (s), 1054 (m), 1023 (m), 971 (m), 918 (w), 849 (m), 803 (w), 735 (s), 642 (m) cm^{-1}. $C_{46}H_{56}ClDyF_6N_2O_9Zn$ (1158.3): calcd. C 47.70, H 4.87, N 2.42; found C 47.71, H 5.05, N 2.38.

[L^{Me2}Zn(Cl)Y/Dy(*(+)*-camph)$_2$(MeOH)], **Λ-Dy/Y:** [ZnL^{Me2}]·2H_2O (93 mg; 0.2 mmol), $DyCl_3$·6H_2O (5.8 mg; 0.016 mmol) and YCl_3·6H_2O (56 mg; 0.183 mmol) were solubilized in 6 mL of methanol. *(+)*-3-(trifluoroacetyl)camphor (97.5 mg; 0.393 mmol) was added to this solution followed by piperidine (32 mg; 0.385 mmol). The resulting pale yellow solution was stirred at room temperature for 30 min. and then transferred in a crystallization tube for slow evaporation of the solution. Pale yellow crystals (62 mg) were collected after several days and washed with methanol. Crystal structure confirmed a crystallographic phase in accordance with that of **Λ-Dy** (Figure S3). IR (ATR): ν = 3402 (vbr, w), 2961 (m), 1662 (s), 1628 (s), 1535 (m), 1539 (m), 1479 (m), 1437 (m), 1393 (w), 1305 (m), 1267 (s), 1243 (w), 1222 (vs), 1199 (vs), 1178 (vs), 1123 (s), 1074 (s), 1051 (m), 1004 (w), 973 (w), 921 (w), 854 (w), 803 (w), 734 (s), 644 (m) cm^{-1}. EDX analysis performed on crystals confirmed the presence of both Y (83.1 wt%, 93.5 mol%) and Dy (16.9 wt%, 10 mol%). A Dy content of 9 mol% was deduced from magnetic behavior (see Figure S6).

[L^{Me2}Zn(Cl)Eu(*(+)*-camph)$_2$(MeOH)], **Λ-Eu**, and [L^{Me2}Zn(Cl)Eu(*(-)*-camph)$_2$(MeOH)], **Δ-Eu** : These complexes have been obtained by same procedure as for the Dy derivatives using $EuCl_3$, 6H_2O. Yield 400 mg (70%); Elemental analysis calcd (%) for $C_{46}H_{56}Cl_1Eu_1F_6N_2O_9Zn_1$ (1148 $gmol^{-1}$): C 48.14, H 4.92, N 2.44; found for **Λ-Eu**: C 47.99, H 4.72, N 2.36; and for **Δ-Eu**: C 48.16, H 4.85, N 2.42. IR (ATR): as for Dy derivatives. XRPD for **Δ-Eu** confirmed a crystallographic phase in agreement with that **Λ-Eu** (Figure S10).

Conflict of Interest

The authors declare no competing financial interest.

Acknowledgements

This work was supported by the French Research Agency (Agence Nationale de la Recherche, reference ANR-09-BLAN-0054-01). Authors are grateful to M. J.-F. Meunier and M. L. Réchignat (LCC) for technical assistance in magnetic data collection.

REFERENCES.

1. D. Gatteschi, R. Sessoli and J. Villain, *Molecular Nanomagnets*, Oxford University Press, Oxford, 2006.
2. M. Faraday, I. Experimental researches in electricity.-Nineteenth series, *Phil. Trans. R. Soc.*, 1846, **136**, 1-20.
3. T. Haider, A Review of Magneto-Optic Effects and Its Application, *Int. J. Electromagn. & and Appl.*, 2017, **7**, 17-24.
4. G. Wagnière and A. Meier, The influence of a static magnetic field on the absorption coefficient of a chiral molecule, *Chem. Phys. Lett.*, 1982, **93**, 78-81.
5. L. D. Barron and J. Vrbancich, Magneto-chiral birefringence and dichroism, *Mol. Phys.*, 1984, **51**, 715-730.
6. P. Kleindienst and G. H. Wagnière, Interferometric detection of magnetochiral birefringence, *Chem. Phys. Lett.*, 1998, **288**, 89-97.
7. M. Atzori, G. L. J. A. Rikken and C. Train, Magneto-Chiral Dichroism: A Playground for Molecular Chemists, *Chem. Eur. J.*, 2020, **26**, 9784-9791.
8. G. L. J. A. Rikken and E. Raupach, Pure and cascaded magnetochiral anisotropy in optical absorption, *Phys. Rev. E*, 1998, **58**, 5081-5084.
9. G. L. J. A. Rikken and E. Raupach, Observation of magneto-chiral dichroism, *Nature*, 1997, **390**, 493-494.
10. K. Taniguchi, M. Nishio, S. Kishiue, P.-J. Huang, S. Kimura and H. Miyasaka, Strong magnetochiral dichroism for visible light emission in a rationally designed paramagnetic enantiopure molecule, *Phys. Rev. Mater.*, 2019, **3**, 045202.
11. M. Atzori, I. Breslavetz, K. Paillot, K. Inoue, G. L. J. A. Rikken and C. Train, A Chiral Prussian Blue Analogue Pushes Magneto-Chiral Dichroism Limits, *J. Am. Chem. Soc.*, 2019, **141**, 20022-20025.
12. C. Train, R. Gheorghe, V. Krstic, L.-M. Chamoreau, N. Ovanesyan, G. L. J. A. Rikken, M. Gruselle and M. Verdaguer, Strong magneto-chiral dichroism in enantiopure chiral ferromagnets, *Nature Mater.*, 2008, **7**, 729-734.
13. R. Sessoli, M.-E. Boulon, A. Caneschi, M. Mannini, L. Poggini, F. Wilhelm and A. Rogalev, Strong magneto-chiral dichroism in a paramagnetic molecular helix observed by hard X-rays, *Nat Phys*, 2015, **11**, 69-74.
14. J. P. Riehl and F. S. Richardson, Circularly polarized luminescence spectroscopy, *Chem. Rev.*, 1986, **86**, 1-16.
15. F. Zinna and L. Di Bari, Lanthanide Circularly Polarized Luminescence: Bases and Applications, *Chirality*, 2015, **27**, 1-13.
16. R. Carr, N. H. Evans and D. Parker, Lanthanide complexes as chiral probes exploiting circularly polarized luminescence, *Chem. Soc.Rev.*, 2012, **41**, 7673-7686.
17. K. Müller, F. Fuchs and F. K. Kneubühl, Partial circular polarization of the spectral thermal emission from ferromagnetic iron, *Phys. Lett. A*, 1977, **64**, 249-250.
18. F. Zinna, C. Resta, S. Abbate, E. Castiglioni, G. Longhi, P. Mineo and L. Di Bari, Circularly polarized luminescence under near-UV excitation and structural elucidation of a Eu complex, *Chem. Comm.*, 2015, **51**, 11903-11906.
19. H. Tsumatori, T. Harada, J. Yuasa, Y. Hasegawa and T. Kawai, Circularly Polarized Light from Chiral Lanthanide(III) Complexes in Single Crystals, *Appl. Phys. Exp.*, 2011, **4**, 011601.
20. J. P. Costes, S. Titos-Padilla, I. Oyarzabal, T. Gupta, C. Duhayon, G. Rajaraman and E. Colacio, Effect of Ligand Substitution around the DyIII on the SMM Properties of Dual-Luminescent Zn–Dy and Zn–Dy–Zn Complexes with Large Anisotropy Energy Barriers: A Combined Theoretical and Experimental Magnetostructural Study, *Inorg. Chem.*, 2016, **55**, 4428-4440.
21. W.-B. Sun, P.-F. Yan, S.-D. Jiang, B.-W. Wang, Y.-Q. Zhang, H.-F. Li, P. Chen, Z.-M. Wang and S. Gao, High symmetry or low symmetry, that is the question - high performance Dy(iii) single-ion magnets by electrostatic potential design, *Chem. Sci.*, 2016, **7**, 684-691.

22. I. Oyarzabal, J. Ruiz, J. M. Seco, M. Evangelisti, A. Camón, E. Ruiz, D. Aravena and E. Colacio, Rational Electrostatic Design of Easy-Axis Magnetic Anisotropy in a ZnII–DyIII–ZnII Single-Molecule Magnet with a High Energy Barrier, *Chem. Eur. J.*, 2014, **20**, 14262-14269.
23. J.-H. Jia, Q.-W. Li, Y.-C. Chen, J.-L. Liu and M.-L. Tong, Luminescent single-molecule magnets based on lanthanides: Design strategies, recent advances and magneto-luminescent studies, *Coord. Chem. Rev.*, 2019, **378**, 365-381.
24. T. D. Pasatoiu, C. Tiseanu, A. M. Madalan, B. Jurca, C. Duhayon, J.-P. Sutter and M. Andruh, Study of the Luminescent and Magnetic Properties of a Series of Heterodinuclear [ZnIILnIII] Complexes *Inorg. Chem.*, 2011, **50**, 5879-5889.
25. A. Ruiz-Martínez, D. Casanova and S. Alvarez, Polyhedral Structures with an Odd Number of Vertices: Nine-Coordinate Metal Compounds, *Chem. Eur. J.*, 2008, **14**, 1291.
26. V. Béreau, V. Jubéra, P. Arnaud, A. Kaiba, P. Guionneau and J.-P. Sutter, Modulation of the Luminescence Quantum Efficiency for Blue Luminophor $\{Al(salophen)\}^+$ by Ester-Substituents *Dalton Trans.*, 2010, **39**, 2070-2077.
27. S. Petoud, G. Muller, E. G. Moore, J. Xu, J. Sokolnicki, J. P. Riehl, U. N. Le, S. M. Cohen and K. N. Raymond, Brilliant Sm, Eu, Tb, and Dy Chiral Lanthanide Complexes with Strong Circularly Polarized Luminescence, *J. Am. Chem. Soc.*, 2007, **129**, 77-83.
28. P. Babu, K. Hyuk Jang, E. Sik Kim, L. Shi and H. Jin Seo, Optical Properties and White-Light Emission in Dy3+-Doped Transparent Oxyfluoride Glass and Glass Ceramics Containing CaF2 Nanocrystals, *J. Korean Phy. Soc.* , 2009, **54**, 1488-1491.
29. J. L. Lunkley, D. Shirotani, K. Yamanari, S. Kaizaki and G. Muller, Extraordinary Circularly Polarized Luminescence Activity Exhibited by Cesium Tetrakis(3-heptafluoro-butylryl-(+)-camphorato) Eu(III) Complexes in EtOH and CHCl3 Solutions, *J. Am. Chem. Soc.*, 2008, **130**, 13814-13815.
30. J. Kumar, B. Marydasan, T. Nakashima, T. Kawai and J. Yuasa, Chiral supramolecular polymerization leading to eye differentiable circular polarization in luminescence, *Chem. Comm.*, 2016, **52**, 9885-9888.
31. R. S. Dickins, J. A. K. Howard, C. L. Maupin, J. M. Moloney, D. Parker, J. P. Riehl, G. Siligardi and J. A. G. Williams, Synthesis, Time-Resolved Luminescence, NMR Spectroscopy, Circular Dichroism and Circularly Polarised Luminescence Studies of Enantiopure Macrocyclic Lanthanide Tetraamide Complexes, *Chem. Eur. J.*, 1999, **5**, 1095-1105.
32. R. Reisfeld, Berlin, Heidelberg, 1973.
33. B. R. Judd, Hypersensitive Transitions in Rare-Earth Ions, *J. Chem. Phys.*, 1966, **44**, 839-840.
34. J.-P. Costes, J.-P. Laussac and F. Nicodème, Complexation of a Schiff base ligand having two coordination sites (N2O2 and O2O2) with lanthanide ions (Ln = La, Pr): an NMR study, *J. Chem. Soc. Dalton Trans.*, 2002, 2731-2736.
35. H. L. Goering, J. N. Eikenberry, G. S. Koermer and C. J. Lattimer, Direct determination of enantiomeric compositions with optically active nuclear magnetic resonance lanthanide shift reagents, *J. Am. Chem. Soc.*, 1974, **96**, 1493-1501.
36. O. Kahn, *Molecular Magnetism*, VCH, Weinheim, 1993.
37. M. Matsushima, K. Wada, Y. Horino, K. Takahara, Y. Sunatsuki and T. Suzuki, Transition-metal(ii) complexes with a tripodal hexadentate ligand, 1,1,1-tris[2-aza-3-(imidazol-4-yl)prop-2-enyl]ethane, exhibiting incomplete total or absolute spontaneous resolution, *CrystEngComm*, 2020, **22**, 458-466.
38. L. Palatinus and G. Chapuis, Superflip, *J. Appl. Cryst.*, 2007, **40**, 786-790.
39. A. Altomare, G. Cascarano, C. Giacovazzo, A. Guargliardi, M. C. Burla, G. Polidori and M. Camalli, SIR92 – a program for automatic solution of crystal structures by direct methods, *J. Appl. Cryst.*, 1994, **27**, 435.
40. P. W. Betteridge, J. R. Carruthers, R. I. Cooper, K. Prout and D. J. Watkin, CRYSTALS, *J. Appl. Crystallogr.*, 2003, **36**, 1487-1487.

SUPPORTING INFORMATION

CONTENTS

Picture 1. Crystals of [L^{Me2}Zn(Cl)Dy((*-*)-camph)$_2$(MeOH)], **Δ-Dy**.

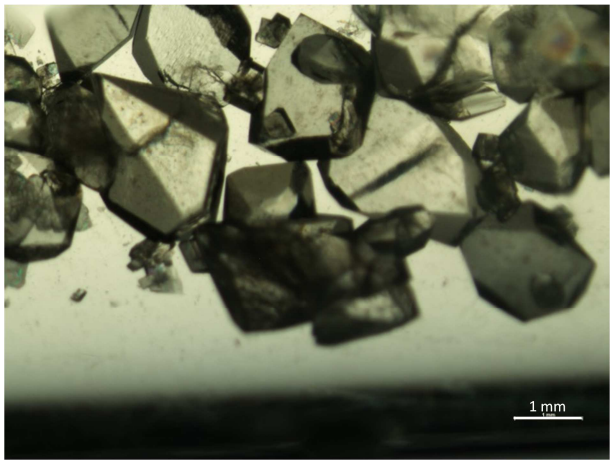

Table S1. Crystal data for **Λ-Dy**, **Δ-Dy**, **Λ-Eu,** and **Λ-Dy/Y**.

Compound	**Λ-Dy**	**Δ-Dy**	**Λ-Eu**	**Λ–Dy/Y**
Empirical formula	$C_{46}H_{56}ClDyF_6N_2O_9Zn$	$C_{46}H_{56}ClDyF_6N_2O_9Zn$	$C_{46}H_{56}ClEuF_6N_2O_9Zn$	$C_{46}H_{56}ClDy_{0.16}F_6N_2O_9Y_{0.84}Zn$
Formula weight (g·mol^{-1})	1158.28	1158.28	1147.74	1096.46
λ (Å)	0.71073	0.71073	1.54180	0.71073
Temperature (K)	100	100	100	110
Crystal system	Orthorhombic	Orthorhombic	Orthorhombic	Orthorhombic
Space group	*P* 2_1 2_1 2_1	*P* 2_1 2_1 2_1	*P* 2_1 2_1 2_1	*P* 2_1 2_1 2_1
a (Å)	13.0607(9)	13.0364(7)	13.0430(2)	13.0472(5)
b (Å)	18.8726(11)	18.8572(11)	18.9020(2)	18.8726(7)
c (Å)	19.3077(13)	19.2842(11)	19.3871(2)	19.2735(9)
Volume (Å^3)	4759.1(5)	4740.6(3)	4779.7(1)	4745.8(3)
Z	4	4	4	4
Calc. Density (g·cm^{-3})	1.616	1.623	1.595	1.534
Absorption coefficient (mm^{-1})	2.197	2.206	11.111	1.913
Theta range for data collection (°)	1.8-35.7	2.1-32.9	3.3-70.4	1.5-30.6
Reflections collected	115603	159374	37407	169605
Independent reflections	18888	16609	9170	14355
R(int)	0.028	0.034	0.033	0.044
Data/restraints/parameters	17290/0/596	15792/0/596	8868/0/596	9542/1/596
Goodness-of-fit	1.09	1.08	1.09	0.97
Refinement on	F	F	F	F^2
Final *R* indices [$I > n\sigma(I)$]	0.0150 (n=3)	0.0125 (n=3)	0.0192 (n=3)	0.0163 (n=2)
Final w*R* indices [$I > n\sigma(I)$]	0.0152 (n=3)	0.0131 (n=3)	0.0228 (n=3)	0.0433 (n=2)
Flack parameter, nb Friedel-pairs	-0.015(2), 8300	-0.009(2), 7333	-0.0135(8), 4090	-0.014(2), 6445
Largest diff. Peak and hole (e Å^{-3})	0.97/-0.91	0.45/-0.46	3.31/-2.99	0.38/-0.19
CCDC reference number	2007105	2007104	2018680	2033959

Figure S1. Asymmetric units for Λ-**Dy** and Δ-**Dy** with numbering scheme.

[L^{Me2}Zn(Cl)Ln(*(+)*-camph)$_2$(MeOH)], **Λ-Dy**	[L^{Me2}Zn(Cl)Ln(*(-)*-camph)$_2$(MeOH)], **Δ-Dy**
ORTEP view (with ellipsoids at the 50%level of probability) of the asymmetric unit	
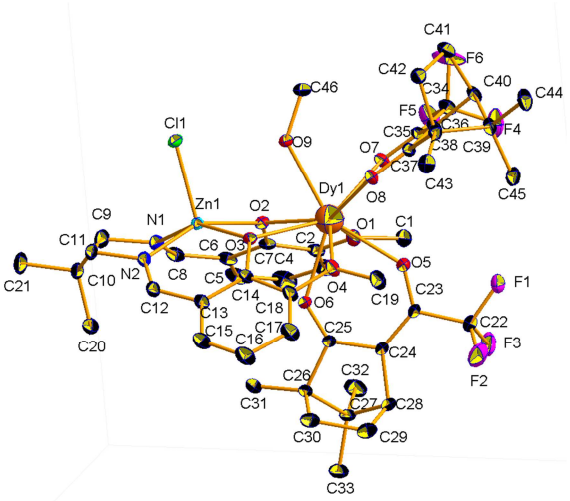	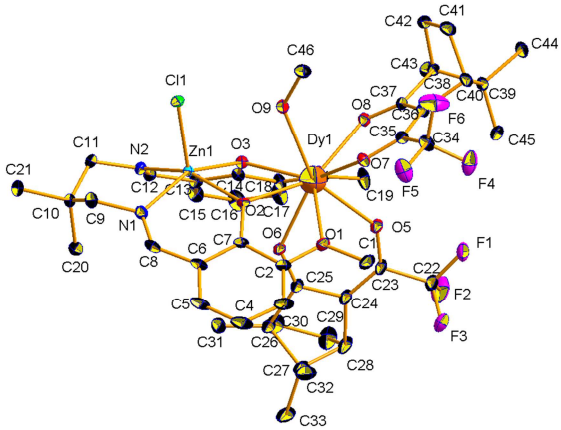
view illustrating the mirror-image relationship of the complexes.	
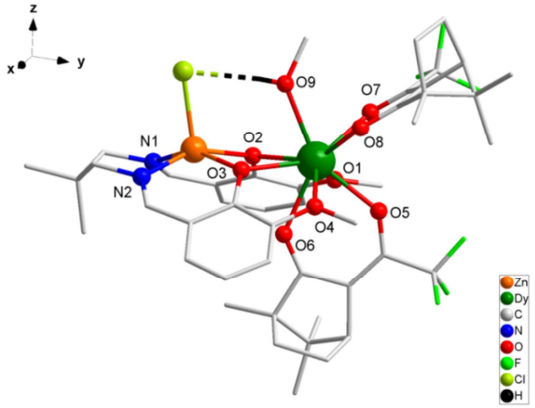	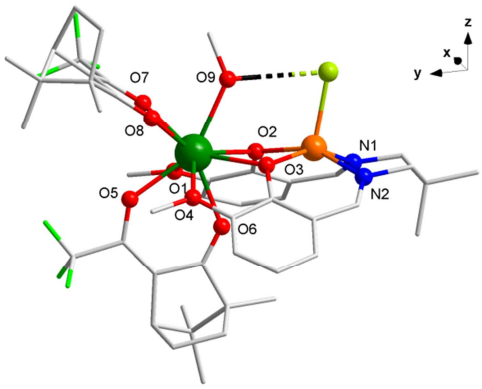

Figure S2. Λ-**Eu** : ORTEP plot (with ellipsoids at the 50% level of probability) of the asymmetric unit with numbering scheme.

[L^{Me2}Zn(Cl)Eu(*(+)*-camph)$_2$(MeOH)], **Λ-Eu**

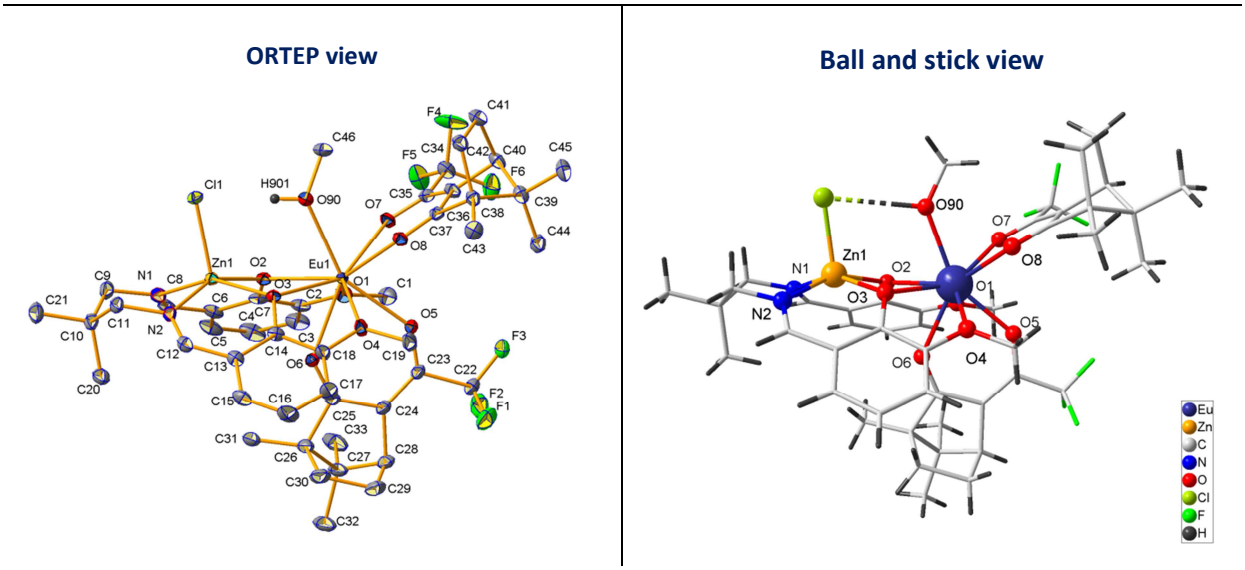

Figure S3. Λ-**Dy/Y** : ORTEP plot (with ellipsoids at the 50% level of probability) of the asymmetric unit with numbering scheme.

[L^{Me2}Zn(Cl)Dy/Y(*(+)*-camph)$_2$(MeOH)], **Λ-Dy/Y**

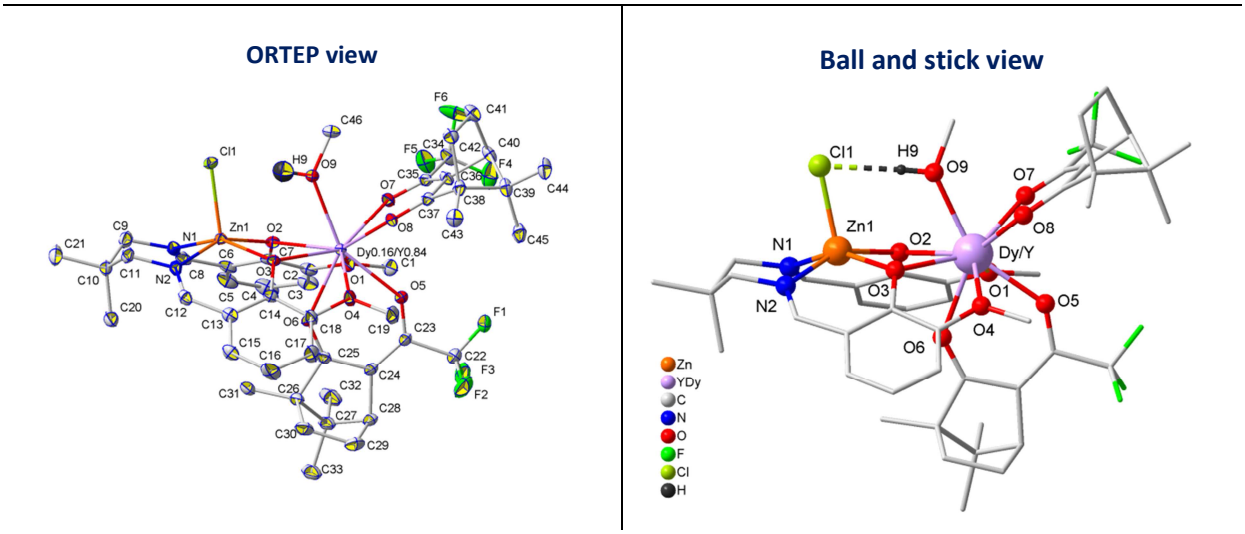

Table S2. Selected bond distances (Å) and angles (°) for **Δ-** and **Λ-Dy**, **Λ-Eu**, and **Λ-Dy/Y** complexes.

		Λ-Dy	**Δ-Dy**	**Λ-Eu**	**Λ-Dy/Y**
Zn1	N2	2.071(1)	2.0674(9)	2.068(2)	2.067(1)
	O2	2.0813(8)	2.0773(8)	2.081(1)	2.080(1)
	N1	2.086(1)	2.084(1)	2.0875(2)	2.086(1)
	O3	2.0907(8)	2.0904(6)	2.091(1)	2.091(1)
	Cl1	2.3116(3)	2.3091(3)	2.3077(5)	2.3087(4)
Dy1	O5	2.323(1)	2.3214(8)	2.352(1)	2.308(1)
	O7	2.3362(9)	2.3314(8)	2.378(1)	2.324(1)
	O6	2.3556(8)	2.3529(8)	2.395(1)	2.350(1)
	O2	2.4069(8)	2.4038(8)	2.438(1)	2.395(1)
	O8	2.407(1)	2.4063(8)	2.447(1)	2.356(1)
	O3	2.4243(8)	2.4231(6)	2.4565(1)	2.4114(9
	O9	2.440(1)	2.4375(8)	2.468(1)	2.420(1)
	O4	2.5370(9)	2.5330(8)	2.550 (1)	2.524(1)
	O1	2.5583(9)	2.5536(8)	2.568(1)	2.548(1)
C1	O1	1.435(2)	1.433(2)	1.435(2)	1.434(2)
C2	O1	1.374(2)	1.373(1)	1.377(3)	1.381(2)
C7	O2	1.326(1)	1.324(1)	1.327(2)	1.328(2)
C14	O3	1.325(1)	1.322(1)	1.324(2)	1.325(2)
C18	O4	1.375(2)	1.375(1)	1.377(2)	1.380(2)
C19	O4	1.438(2)	1.436(1)	1.439(2)	1.442(2)
C23	O5	1.280(2)	1.280(1)	1.277(2)	1.281(2)
C25	O6	1.242(1)	1.238(1)	1.239(2)	1.239(2)
C35	O7	1.273(2)	1.274(1)	1.274(2)	1.276(2)
C37	O8	1.246(2)	1.245(1)	1.244(2)	1.245(2)
C46	O9	1.431(2)	1.428(1)	1.432(2)	1.429(2)
Cl1	O9	3.022(1)	3.0219(8)	3.025(1)	3.022(1)
Cl1	H9	2.2273(3)	2.1898(3)	2.1764(4)	2.1600(4)
O2	Zn1	80.49(3)	67.77(3)	80.95(5)	80.22(4)
	O3	80.49(3)	67.83(3)	67.20(4)	67.98(3)
O2	Dy1				
	O3				
O2					

Table S3: SHAPE Analysis for the ML9 coordination sphere of the Ln ions.[1]

CSAPR-9 Spherical capped square antiprism
MFF-9 Muffin

[ML9]	CSAPR-9 (C_{4v})	MFF-9 (Cs)
Δ-Dy	1.396	**1.391**
Λ-Dy	1.399	**1.398**
Λ-Dy/Y	**1.356**	1.357
Λ-Eu	1.545	**1.457**

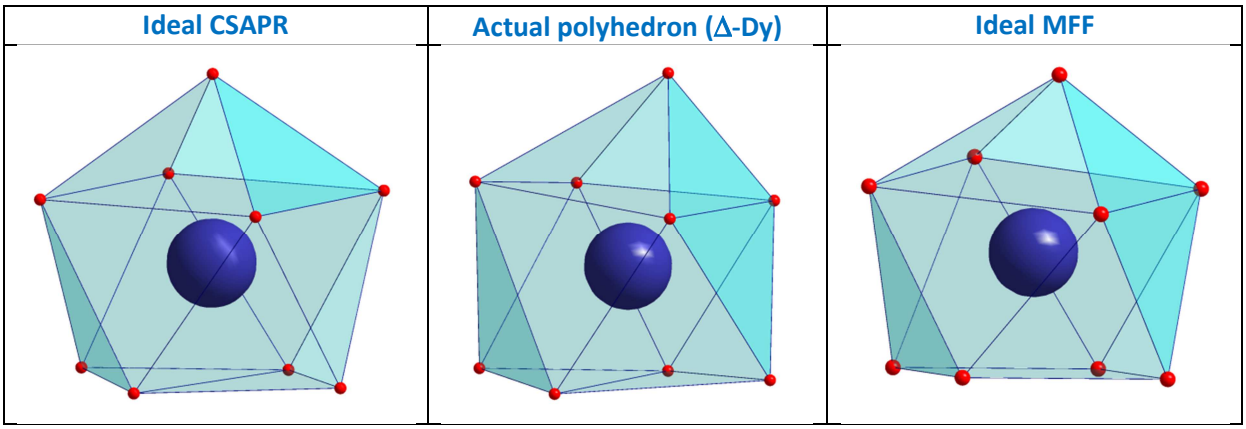

Figure S4. Solid-state UV-vis spectra for ZnL^{Me2} and $[L^{Me2}Zn(Cl)Dy((+/-)\text{-camph})_2(MeOH)]$ complexes.

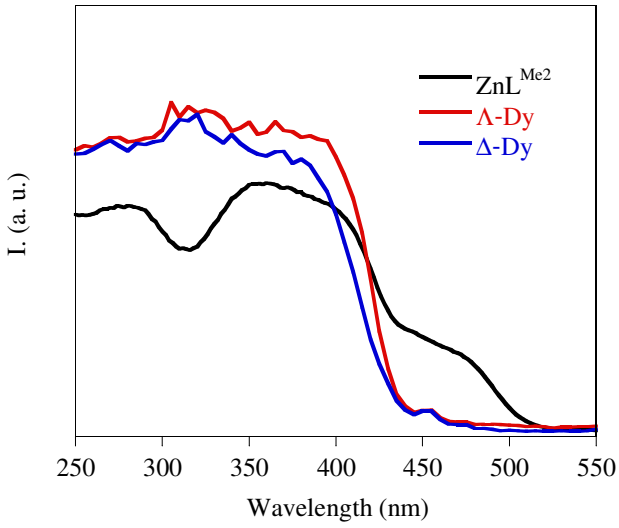

[1] Llunell, M.; Casanova, D.; Cirera, J.; Alemany, P.; Alvarez, S.; SHAPE: Program for the stereochemical analysis of molecular fragments by means of continuous shape measures and associated tools 2.1 ed.; University of Barcelona: Barcelona, 2013.

Figure S5. Magnetic behaviors for **Dy** complex.

Magnetic behavior is independent of the chirality therefore a full set of magnetic behavior has been collected only for **Λ-Dy**. The magnetic purity of the Δ enantiomer was confirmed by susceptibility values at 300 K (found $\chi_M T$ = 14.10 $cm^3mol^{-1}K$) and AC versus *T* trace with frequency of 1 kHz (shown below) that was found identical to **Λ-Dy**.

DC studies: The temperature dependence of $\chi_M T$ for **Λ-Dy** (Fig. S5a) is in agreement with the behavior expected for an isolated Dy(III) ion. The value found at 300 K is 14.15 $cm^3mol^{-1}K$ and reaches 11.41 $cm^3mol^{-1}K$ at 4 K. Magnetization versus field at 2 K (b) reaches as value of 5.35 μ_B under 5 T.

(a)

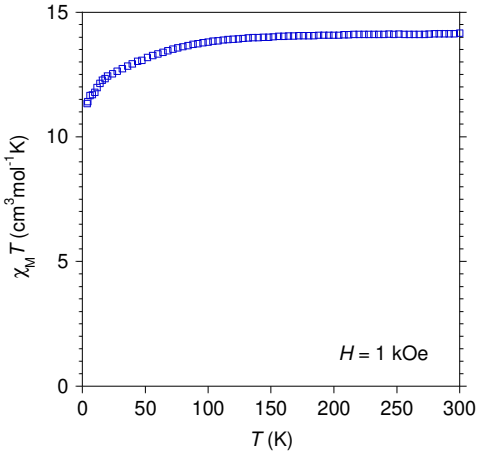

(b)

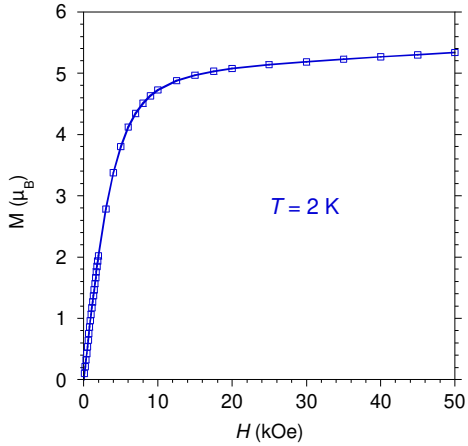

AC studies: AC magnetic susceptibility as a function of temperature recorded without an applied filed is shown in (c). An out-of-phase component, χ_M'', was found below 15 K and lower temperature behavior indicated other relaxation processes become active. Application of an external DC field allowed to drastically reduce these contributions but not to fully cancel them even when a field of 3 kOe (d). Since the $\chi_M'' = f(T)$ for different AC frequencies obtained with H_{DC} = 1 kOe display well defined maxima, a full data set was collected (e). The temperature dependence of the relaxation time between 3.8 and 10 K (f) was obtained by analyzing the $\chi_M'' = f(\nu)$ for different temperatures with an extended Debye model. The linear variation of $\tau = f(1/T)$ between 10 and 6.5 K was fitted assuming a thermally activated process yielding U_{eff}/k_B = 42 K with $\tau_0 = 1.4 \times 10^{-6}$ s (dotted blue line). A modelling over the entire temperature range (3.8 to 10 K, red line) was possible considering contributions from the Orbach and Raman relaxation processes ($\tau = \tau_0 e^{Ueff/kT} + 1/(RT^n)$). The values of the adjustment parameters are U_{eff}/k_B = 53 ± 9 K, τ_0 = 0.8 ± 2 $\times 10^{-8}$ s, R = 0.2 ± 0.1 s^{-1}, n = 4.9± 0.4.

(c)

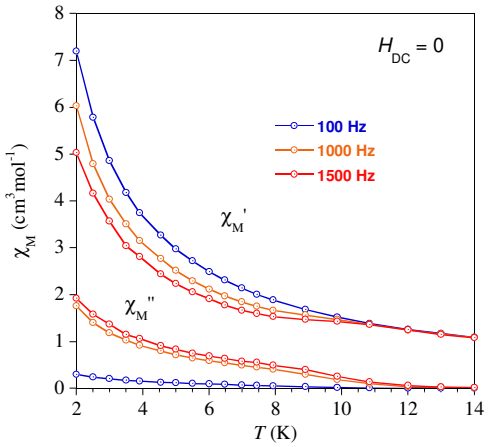

(d)

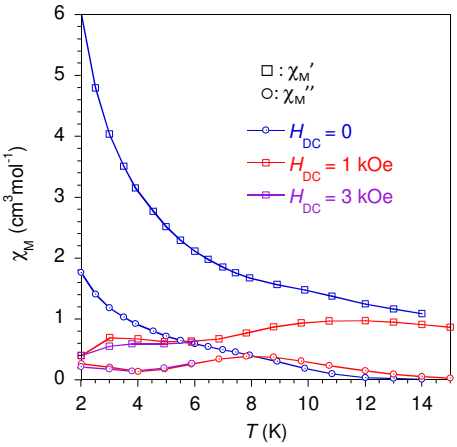

(e)

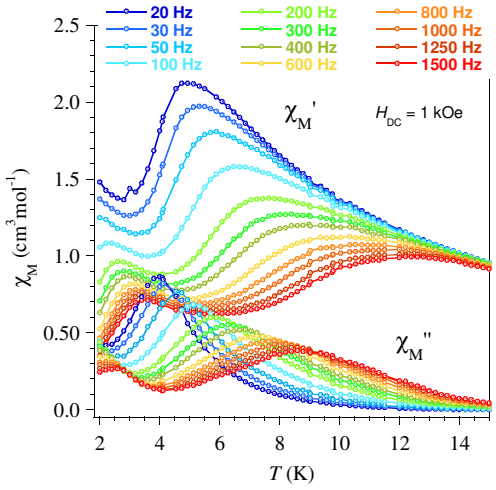

(f)

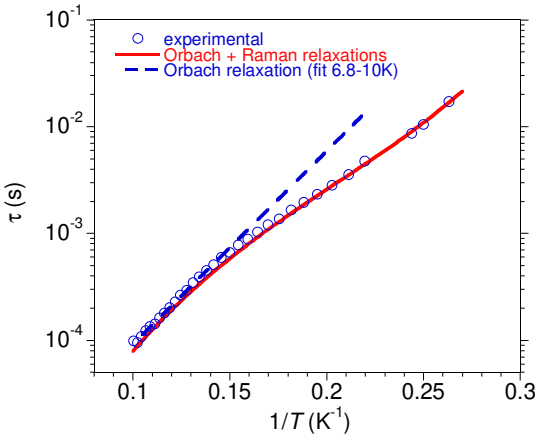

Figure S5g shows the χ_M'' = *f*(T) trace for Δ-**Dy** under H_{DC} = 1 kOe and for ν = 1 kHz which confirms a behavior identical to that of the Λ-Dy enantiomer.

(g)

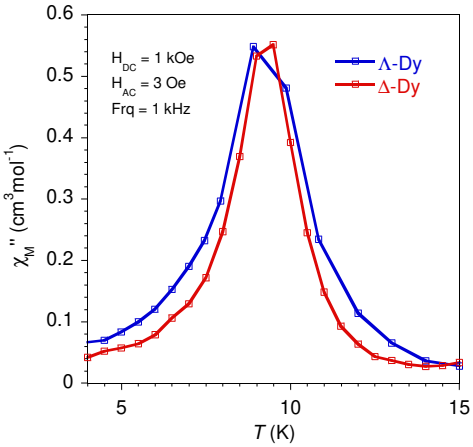

Figure S6. Magnetic behaviors for [L^{Me2}Zn(Cl)Y/Dy((*+*)-camph)$_2$(MeOH)], **Λ-Dy/Y**.

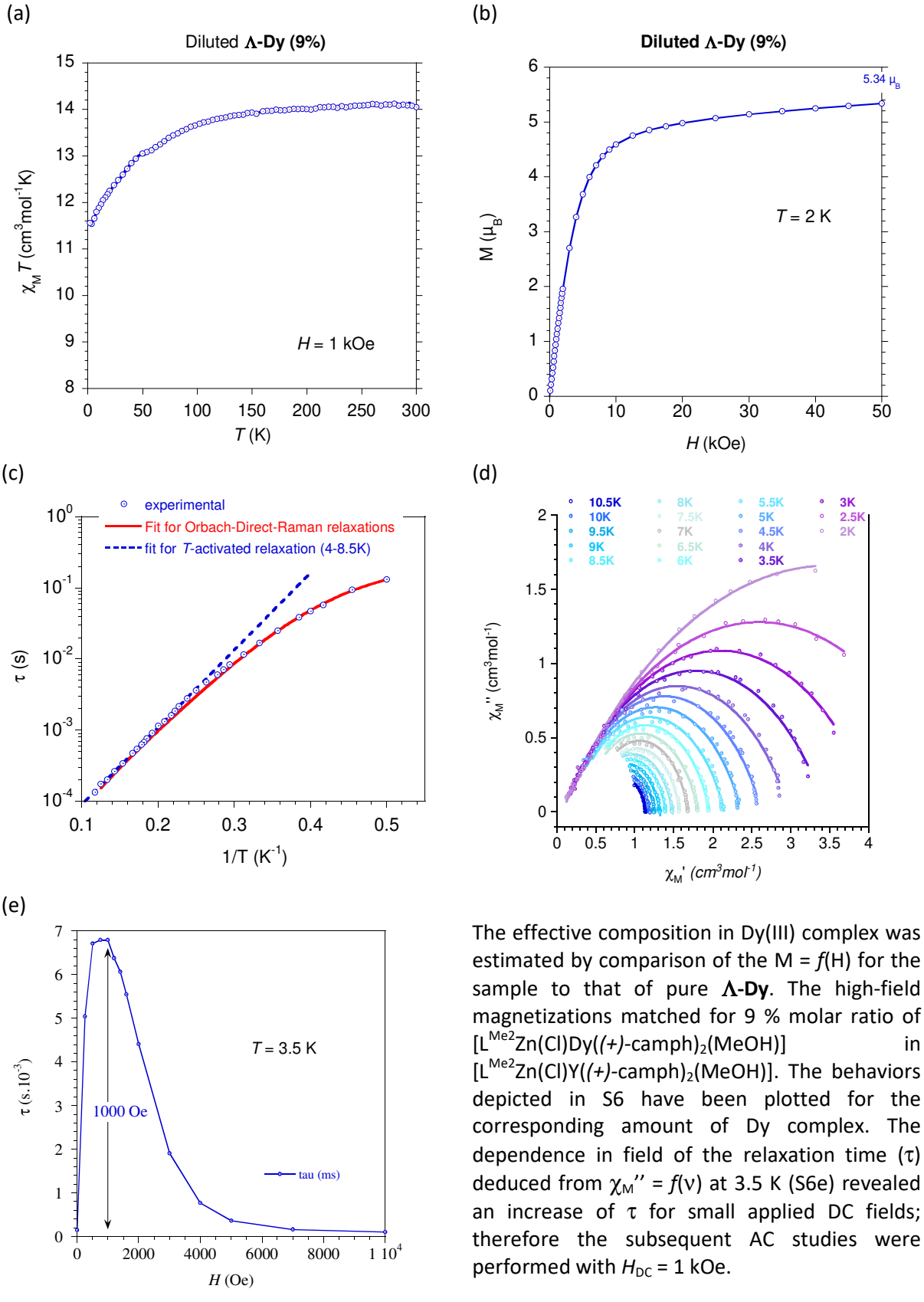

The effective composition in Dy(III) complex was estimated by comparison of the M = *f*(H) for the sample to that of pure **Λ-Dy**. The high-field magnetizations matched for 9 % molar ratio of [L^{Me2}Zn(Cl)Dy((*+*)-camph)$_2$(MeOH)] in [L^{Me2}Zn(Cl)Y((*+*)-camph)$_2$(MeOH)]. The behaviors depicted in S6 have been plotted for the corresponding amount of Dy complex. The dependence in field of the relaxation time (τ) deduced from χ_M'' = *f*(ν) at 3.5 K (S6e) revealed an increase of τ for small applied DC fields; therefore the subsequent AC studies were performed with H_{DC} = 1 kOe.

Picture 2: Crystals (size 300-800 µm) and powders (crushed crystal) on the cold stage for micro-photoluminescence studies.

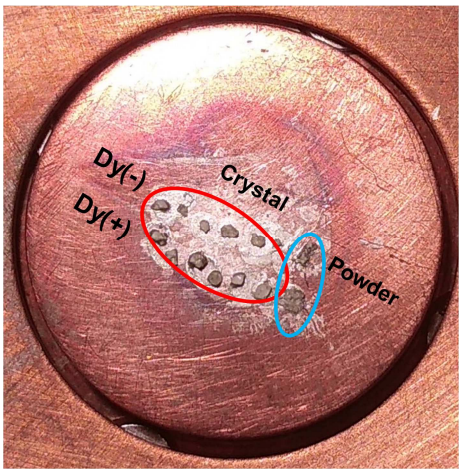

Figure S7. (a) Temperature dependent emission of a **Δ-Dy** crystal. Blue lines: left-handed circular (LHC) polarization; red lines: right-handed circular (RHL) polarization. (b) Temperature dependence of the deduced dissymmetry factor g_{lum}.

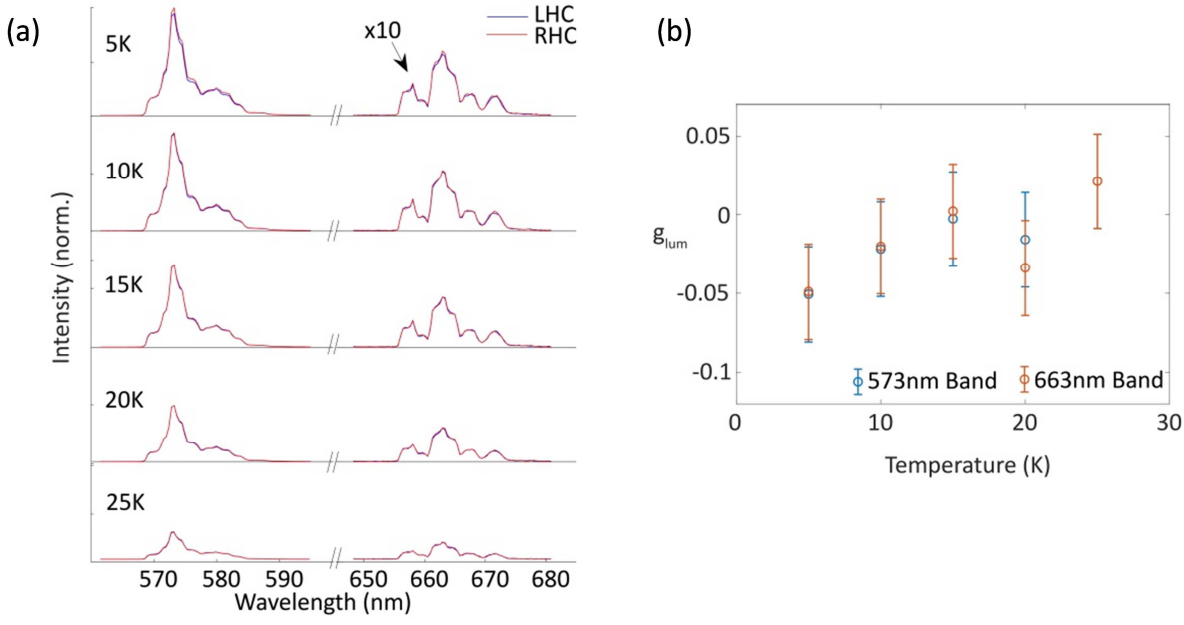

Figure S8. Temperature dependent emission and g_{lum} for a **Λ-Eu** (a, b), and a **Δ-Eu** (c, d) crystal (blue lines: left-handed circular (LHC) polarization; red lines: right-handed circular (RHL) polarization); (e) emission spectrum at 5 K (**Δ-Eu**).

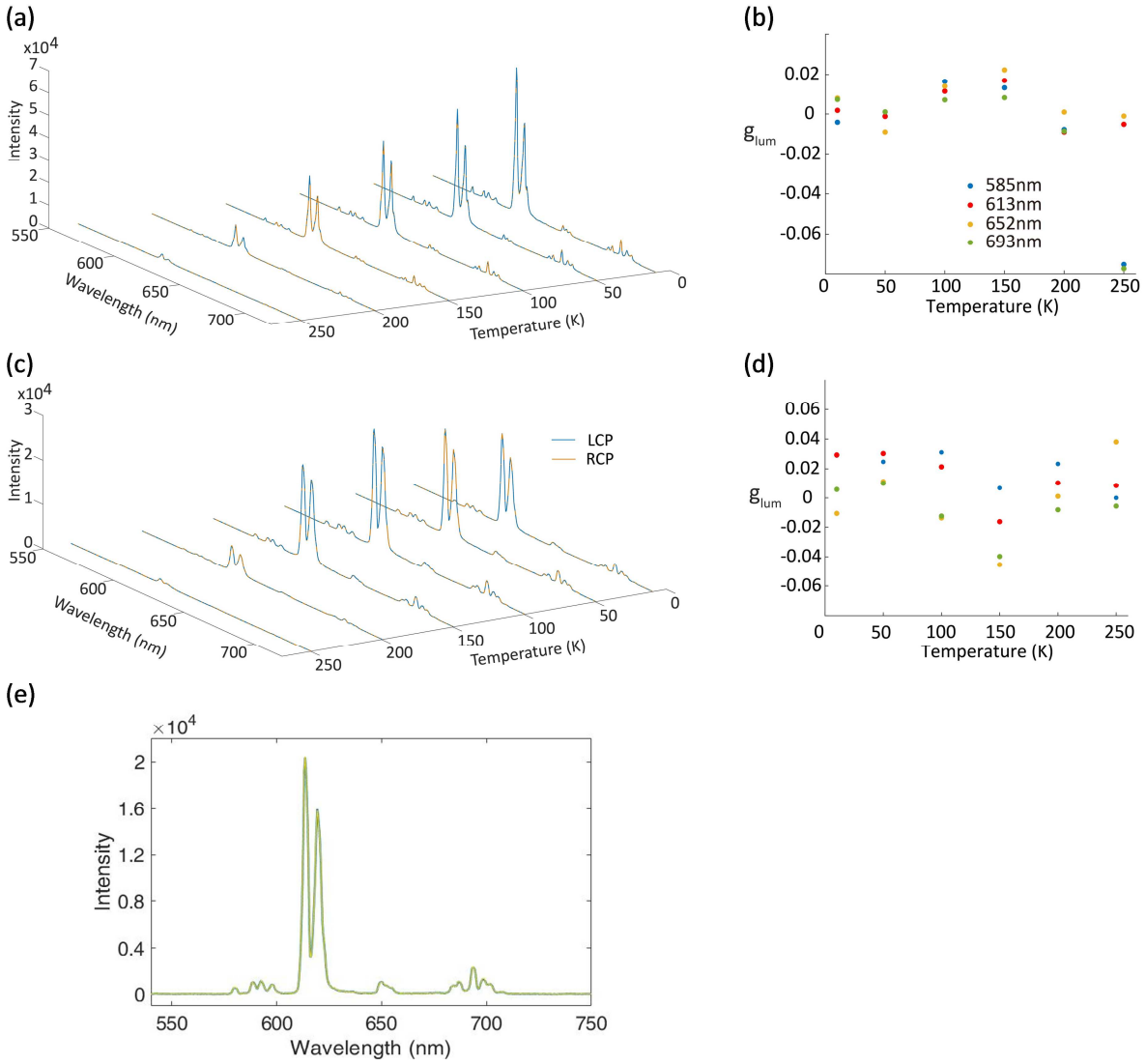

Figure S9. Angular distribution of the emission (bands at 573-nm and 663-nm) recorded at 5K, and temperature dependent variation of the dissymmetry factor g_{lum} for a crystalline powder of *(left)* **Λ-Dy** and *(right)* a **Δ-Dy** crystal. The grey portions correspond to the angles not collected by the objective (outside the numerical aperture).

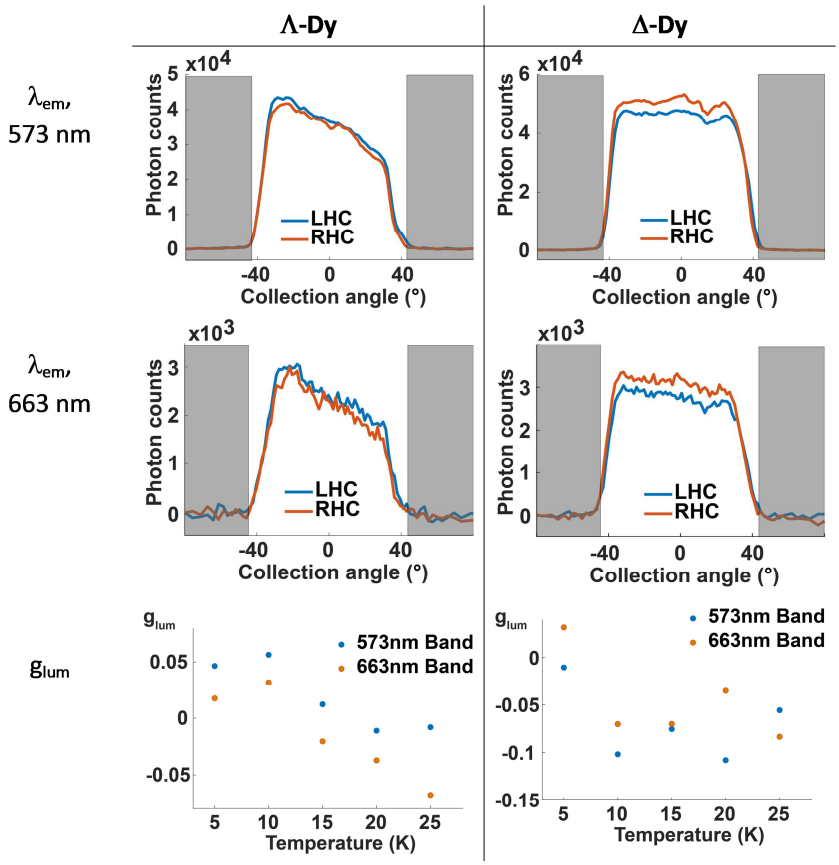

Figure S10. X-Ray Powder Diffraction (*XRPD*) at 295 K for **Λ-Dy** , **Δ-Dy**, **Λ-Eu**, and **Δ-Eu.**